Enzymatic reduction of oxygen by small laccase. A rapid freeze-quench EPR study

Nami, F.

Chapter 4

A Rapid Freeze-Quench Multi-Frequency EPR Study of an Intermediate in the Enzymatic Reduction of Oxygen by Small Laccase.

The T1D and T1D Y108F mutants

In this chapter multi-frequency EPR spectroscopy is combined with the rapid freeze-quench technique to trap and characterize intermediates formed during the reaction of fully reduced T1D and T1D Y108F SLAC with oxygen on the time scale of milliseconds. A single paramagnetic intermediate is detected for T1D SLAC. The analysis of EPR data at 9, 94 and 275 GHz of RFQ samples unambiguously indicates that this intermediate concerns a biradical, which consists of the T2 Cu and the tyrosyl 108 radical. The spins are found to be coupled by an exchange interaction of 12 ± 1 GHz at a distance of 5.7 ± 0.1 Å. This distance is in excellent agreement with structural data. For Y108F T1D SLAC, there was no sign of a biradical intermediate during the reoxidation process on the time scale of milliseconds to seconds, which confirms the crucial role of tyrosine 108 in the reaction of T1D SLAC with molecular oxygen. For the double mutant, we observe an intermediate with a small contribution of a radical, which is tentatively assigned to a tryptophanyl radical based on its small g-anisotropy.

4.1 Introduction

Laccases belong to the group of multicopper oxidase (MCO) enzymes, which catalyze the reduction of oxygen to water while oxidizing a wide variety of substrates. These enzymes contain at least four copper atoms: a mononuclear type 1 (T1) copper, which receives electrons from a substrate and transfers these to a trinuclear copper center (TNC), where oxygen binds and gets reduced[1,2]. The TNC consists of a type 2 (T2) copper and a binuclear type 3 (T3) copper. The T1 Cu is characterized by an intense absorption band at ~600 nm and an EPR signal with a small parallel hyperfine coupling of about 200 MHz. The T2 Cu shows no appreciable absorption in the visible and a larger parallel hyperfine coupling of about 500 MHz. The T3 Cu's exhibit an absorption shoulder at ~330 nm but do not give rise to an EPR signal. The molecular mechanism of O_2 reduction has been studied in several MCO's and, according to the proposed mechanism[3,4,5], the reaction with the fully reduced enzyme proceeds via two sequential two-electron steps, the first generating a peroxide intermediate (PI) and the second generating the native intermediate (NI). An open issue is whether the proposed mechanism applies to all MCO subfamilies, which are structurally different, stem from different sources and function under different conditions.

Some years back, an MCO called small laccase (SLAC) has been identified when searching the genome of *Streptomyces coelicolor* for the presence of copper proteins[6]. Characterization of the protein revealed that SLAC represents structural and reactivity features distinct from those of other laccases. However, the active-site morphology of SLAC, which involves a T1 Cu and a TNC, is the same as for other MCO's. The SLAC consists of only two cupredoxin-like domains and it is active as a homotrimer, contrary to the more common three-domain MCO's (3dMCO's), which are active in monomeric form.

Remarkably, the T1 Cu depleted (T1D) SLAC is still able to complete the reduction of O_2 to H_2O, while for 3dMCO's in the absence of the T1 Cu, the reduction of O_2 stops at the peroxide level. Reaction of the reduced T1D SLAC with oxygen results in the formation of an intermediate detected by electron paramagnetic resonance (EPR) on the time scale of minutes[7]. The half-field EPR signal observed for this intermediate was indicative of a triplet state. The EPR observations on the SLAC intermediate led to the hypothesis of a biradical, which originates from two exchange-coupled spins, one localized on the T2 Cu and the other one on an amino-acid-derived radical. The distance between the two electrons was estimated to be approximately 5 Å from the intensity of the half-field signal.

Stopped-flow experiments on T1D SLAC showed the immediate appearance of an absorption band around 420 nm, after mixing the reduced enzyme with oxygen. Based on the similar decay rates observed by EPR spectroscopy for the biradical intermediate and observed for the 420 nm optical transition, it was concluded that the EPR and optical signals derive from the same species. The appearance of the 420 nm band was attributed to the formation of a tyrosyl radical. This proposal was later supported by the crystal structure of SLAC[8], which showed the presence of a tyrosine residue (Y108) whose oxygen is 4.5 Å away from the T2 Cu (figure 1). When Tyr 108 was replaced with alanine (Y108A) or phenylalanine (Y108F) by site-directed mutagenesis, no biradical signal was observed on the time scale of minutes[9]. As the O_2 reduction to H_2O requires four electrons and each copper center provides one electron, in the absence of T1 Cu an insufficient number of electrons is available to complete the reaction. For T1D SLAC the fourth electron required to complete the reduction is proposed to be provided by a tyrosine residue[9] to prevent the generation of reactive oxygen species, which might damage the enzyme.

Tyrosyl radicals are known to play a catalytic role in many metalloproteins[10,11,12,13,14,15] such as, galactose oxidase[16,17], ribonucleotide reductase[18], photosystem II[19] and prostaglandin H synthase[20,21]. Tyrosyl radicals have been observed in the reaction of cytochrome *c* oxidase with hydrogen peroxide[22,23], but their role in the mechanism of O_2 reduction is a matter of debate. Recently, Yu and co-workers[24] have detected a tyrosyl radical in a functional oxidase model in myoglobin called F33Y-Cu_BMb during both H_2O_2 and O_2 reaction. As SLAC is to date the only MCO in which the involvement of a tyrosyl radical in the enzymatic reaction has been reported[7,9], investigation of the mechanism of SLAC, a 2dMCO, is of great interest to see the possible mechanistic differences and similarities with the 3dMCO's.

The reduction of O_2 by SLAC has been studied by transient optical absorption spectroscopy on the time scale of milliseconds.[7] So far no EPR study of SLAC intermediates with such a time resolution has been reported. The EPR investigation of paramagnetic enzymatic intermediates, which involve paramagnetic species such as amino-acid-derived radicals or transition metal ions, presents the advantage of higher selectivity compared to the investigation by optical spectroscopy. An EPR spectrum provides insight into the nature of the paramagnetic center, its conversion during the reaction and its interaction with the local environment.

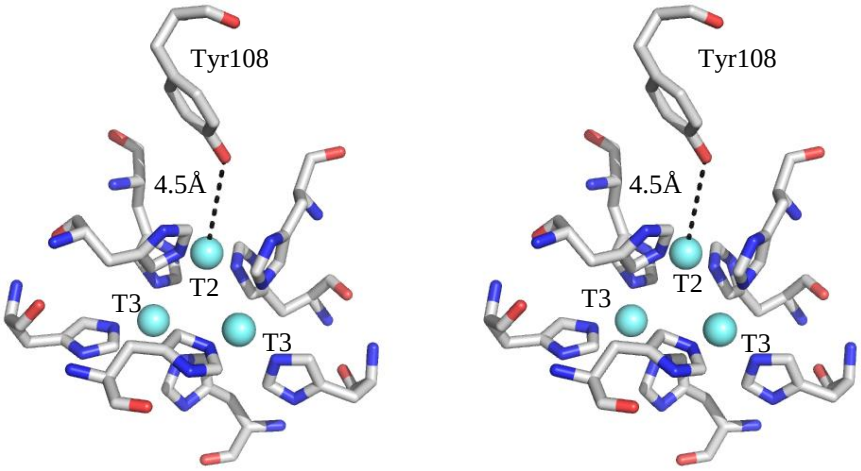

Figure 4.1. The stereo view of the trinuclear Cu cluster of the SLAC active site with the coordinated histidines and the Tyr108 (PDB: 3CG8). Color code: Cu, cyan; C, gray; N, blue; O, red.

The previous EPR studies[7] of the SLAC-catalyzed reaction were performed on samples prepared by manual mixing for which the dead time is at least 30 seconds. The EPR spectrum of the intermediate was extracted as the difference of the spectra corresponding to different reaction times. With such a time resolution, it was only possible to follow the decay of the intermediate. For many enzymatic systems, it has been reported that the trapped radical intermediate on the time scale of seconds/minutes differs from the initially generated transient radical[11]. The initial radical, which is mechanistically more interesting, can migrate for instance to a more stable location. Therefore, it is important to trap the intermediates on the sub-seconds time scale in order to characterize mechanistically important species by EPR.

Rapid freeze-quench (RFQ) is a proven method[25,26] to trap the intermediates on the time scale of milliseconds. In RFQ the reaction components are rapidly mixed and after a certain time the reaction is instantly quenched in a

cryomedium. The mechanism of a large number of enzymatic reactions, in particular copper- and iron-containing enzymes, has been studied by RFQ EPR techniques at the classical 9.5 GHz microwave frequency[26,27,28,29,30]. In many cases, due to the complexity of EPR signals for enzymatic intermediates, it is essential to perform EPR experiments at a number of different microwave frequencies. Higher microwave frequencies in combination with higher magnetic fields provide enhanced resolution, which facilitates the assignment of EPR spectra for organic radicals with small g anisotropy and for multiple paramagnetic species. Higher microwave frequencies also enable a multi-frequency approach, which is useful for systems with S>½. An additional advantage of high-frequency spectrometers equipped with a single-mode cavity is that only sub-microliter sample volumes are needed, which is particularly relevant for precious materials like proteins of which often limited quantities are available. In chapter 3, we have demonstrated a systematic approach to combine the RFQ technique with multi-frequency EPR up to 275 GHz. For each point in time, one RFQ sample suffices for EPR experiments at all frequencies.

In this chapter we make use of RFQ multi-frequency EPR to trap and characterize paramagnetic intermediates formed during the reaction of fully reduced T1D and T1D Y108F SLAC with oxygen on the time scale of milliseconds. For T1D SLAC, a biradical intermediate has been detected, which includes tyrosine 108, and which could be completely characterized by the combined analysis of EPR data at 9, 94 and 275 GHz. For Y108F T1D SLAC, no biradical intermediate is involved in the reoxidation process. A small contribution of a radical was detected, most probably a tryptophanyl radical.

4.2 Materials and methods

4.2.1 Protein isolation. The T1D (C288S) and T1D Y108F SLAC were isolated from *E. coli* cultures harboring the pET20b overexpression plasmid as previously described[6]. The purity of the preparations was checked by SDS PAGE. The protein was stored in 10mM phosphate buffer pH 7.2 containing 0.1 M NaCl at −80 °C until required for use. Protein concentration was determined by absorption spectroscopy using an extinction coefficient of 48 mM^{-1} cm^{-1} at 280 nm.

4.2.2 Chemicals. All chemicals were of analytical grade, purchased from Sigma-Aldrich and used without further purification.

4.2.3 EPR measurements. The 9.5 GHz spectra were recorded on an ELEXSYS E680 spectrometer (Bruker BioSpin GmbH) equipped with a He-flow ESR900 Cryostat (Oxford Instruments) and a standard TE102 cavity.

The 94.1 GHz spectra were recorded on a Bruker ELEXSYS E680 spectrometer equipped with a He-flow CF935 Cryostat (Oxford Instruments) and a home-built probe head with a single-mode cavity specially designed for continuous-wave (cw) measurements.

The 275.7 GHz spectra were recorded on a home-built spectrometer[31] equipped with a He-flow CF935 Cryostat (Oxford Instruments) and a home-built probe head with a single-mode cavity specially designed for cw measurements[32].

All 94 and 275 GHz spectra were recorded after temperature stabilization of approximately two hours and the actual temperature of the cavity was verified by a calibrated Cernox resistor (Lake Shore Cryotronics) attached to it.

4.2.4 Rapid-freeze-quench device. The RFQ experiments were performed using an Update Instrument System 1000 Chemical/Freeze Quench Apparatus

with a Model 1019 syringe ram and a Model 715 ram controller. The reactant syringes are connected to the mixer via the coupling hoses in a T-shaped inlet arrangement. The mixing starts when the two reagents meet and is considered to be complete before the reaction mixture reaches the reactor. The reaction takes place in the reactor, which connects the outlet of the mixer to the nozzle. The reaction time is tuned by variation of the length of the reactor and of the velocity of the syringe plungers (see figure 1.3).

We use isopentane as cryogenic medium at the temperature of –135 to –140 °C. Pre-cooled nitrogen gas is used to maintain the temperature of the isopentane bath during the sample preparation. The temperature of the bath is monitored with a thermometer equipped with a Type K thermocouple (OMEGAETTE, model HH308). The isopentane bath is continuously stirred to ensure a homogeneous temperature. A glass tube (Duran, 12 ml) is filled with cold isopentane and equilibrated in the isopentane bath. The opening of the tube is covered to minimize warming up. Once the isopentane in the glass tube reaches the desired temperature, we start the sample preparation. The reagents are rapidly mixed and the reaction mixture is sprayed through the nozzle into the isopentane in the glass tube, which causes instantaneous quenching of the reaction. The reported reaction times include the dead-time (5 ms) of the RFQ device.

4.2.5 RFQ sample preparation. To prepare samples using the RFQ technique, the enzyme was anaerobically reduced by addition of a slight excess of anaerobically prepared sodium dithionite (DT) in a glovebox. The reduction was monitored on a mini UV-Vis spectrometer (Ocean Optics) as decrease of the 330 nm band for T1D SLAC, which completely disappears for a fully reduced T1D SLAC. The excess of DT was removed in the glovebox using a 10K Amicon centrifugal filter from Millipore. Before loading the reduced

enzyme into the RFQ syringe, the UV-Vis spectrum was recorded to ensure that no DT is remained in the solution (DT absorbs at 315 nm, $\varepsilon_{315} = 8\ mM^{-1}cm^{-1}$). To the reduced T1D SLAC a 40 µM anaerobically prepared $MnCl_2$ solution was added as an internal standard. The syringe assemblies for the enzyme were made rigorously anaerobic in the glovebox one day prior to the experiment. The samples were prepared by 1:1 mixing of the reduced enzyme with oxygen-saturated phosphate buffer (100mM, pH 6.8). The mixing was conducted at room temperature and the reaction mixture was sprayed into cold isopentane. Frozen particles were then packed into a 3mm (i.d.) EPR tube using the sucking method[33], which we developed recently, and a steel rod. The RFQ/EPR samples for high-frequency measurements were prepared according to the method described in chapter 3. Using this method, one RFQ sample for each point in time suffices for EPR experiments at multiple microwave frequencies.

The samples with a reaction time of more than one second were frozen in a different way. The reactants were mixed by the RFQ setup and the reaction mixture was directly injected into an EPR tube and frozen on dry ice.

The unreacted sample was prepared by freezing the reduced T1D SLAC solution containing Mn(II) in an EPR tube on dry ice inside the glovebox.

4.3 Results

4.3.1 Reoxidation of T1D SLAC

The X-band EPR spectra at 40 K of freeze-quench samples of pre-reduced T1D SLAC reacted with oxygen for different times between 8 ms and 10 seconds are presented in figure 4.2. All the spectra are normalized according to the Mn (II) signal to eliminate the effect of the packing factor and of the amount of sample in each EPR tube. The spectrum of the unreacted sample, which consists of the

Mn(II) signal and a small signal of unreduced Cu, was subtracted from all the spectra. The samples were also measured at lower temperatures and the EPR spectra were found to be essentially identical to those at 40 K. At temperatures below 10 K and high microwave power, the spectra also contain a half-field signal around 160 mT (figure 4.12). The spectra in figure 4.2 show a broad and structured band, which initially extends from 285 to 360 mT. Not much changes up to reaction times of seconds, when a signal appears at about 272 mT, which has the characteristics of the low-field hyperfine component of the T2 Cu spectrum (figure 4.13, as purified T1D SLAC). The spin quantification is given in the inset of figure 4.2. The number derives from double integration of the EPR spectrum and normalization to the double integral of the spectrum of the resting form of T1D SLAC. The spectrum of the intermediate from 8 ms to 10 s corresponds to 1.05, 1.50, 1.88, 1.8 and 1.75 spins, respectively.

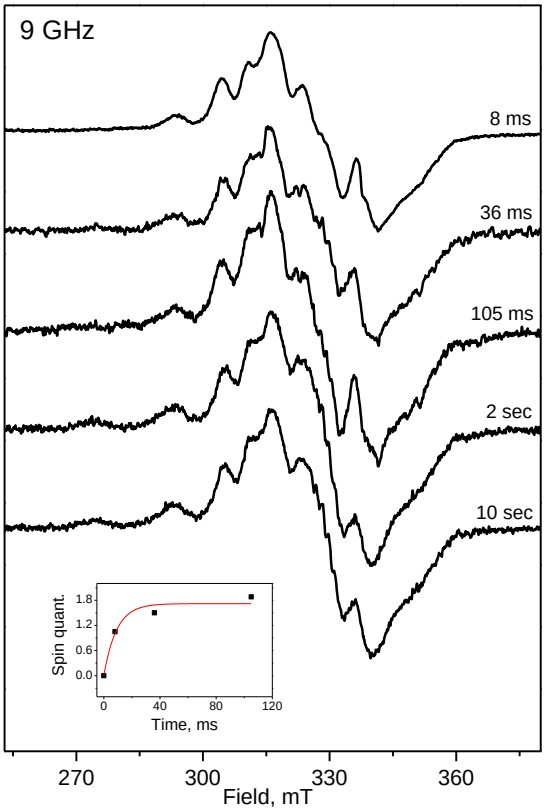

Figure 4.2. The cw EPR spectra at X-band of freeze-quench samples of reduced T1D SLAC reacted with oxygen for different times. The inset shows the spin quantification derived from double integration of the EPR spectrum and normalization to the double integral of the spectrum of the resting form of T1D SLAC. Enzyme and oxygen concentration are 350 μM (500 μM for the 8 ms sample) and 650 μM, respectively, both in 100 mM sodium phosphate buffer, pH 6.8. EPR measurements: microwave frequency 9.5 GHz, T = 40 K, microwave power 0.16 mW and modulation amplitude 0.5 mT.

The measurement of the unreacted reduced enzyme shows that there is no intermediate present in this sample (t = 0). The monoexponential fit to the

points with the reaction time up to 105 ms yields the apparent rate constant of 110 ± 22 s^{-1}. Taking into account the concentration of oxygen, 650 μM, the second order rate constant would be 1.7 ± 0.3× 10^5 $M^{-1}s^{-1}$.

The EPR spectrum of the RFQ sample of reduced T1D SLAC reacted with oxygen for 8 ms was also measured at 94 and 275 GHz. The spectra are presented in figures 4.3 and 4.4. The 94 GHz spectra consist of a broad band, which extends from 3.19 to 3.27 T, and three features with a linewidth of approximately 15 mT between 3.28 and 3.35 T. The small features above 3.35 T result from the imperfect subtraction of the Mn (II) signal. The intensity of the signals around 3.25 and 3.28 T increases relative to the 3.32 T signal when lowering the temperature from 40 K to 15 K (figure 4.3).

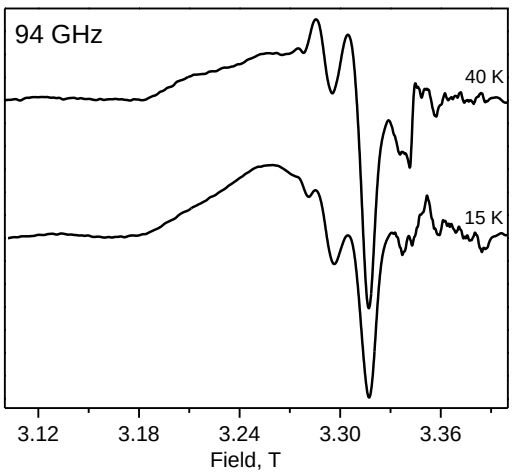

Figure 4.3. Cw EPR spectra at 94.1 GHz and temperatures of 15 and 40 K of the RFQ sample of pre-reduced T1D SLAC reacted with oxygen for 8 ms. Enzyme and oxygen concentration are 500 μM and 650 μM, respectively, both in 100 mM sodium phosphate buffer, pH 6.8. EPR measurements: modulation amplitude 1.2 mT and microwave power 80 μW and 50 μW for the spectra at 40 and 15 K, respectively.

The 275 GHz spectrum (figure 4.4) shows less structure compared to the spectra at 9 and 94 GHz. It consists of a broad signal with three features, which extends from 9.45 to 9.8 T. The six-line Mn(II) signal and an organic-radical-like signal show up around 9.85 T. The measurements on an empty cavity suggest that the signal at 9.6 T originates from an impurity in the cavity.

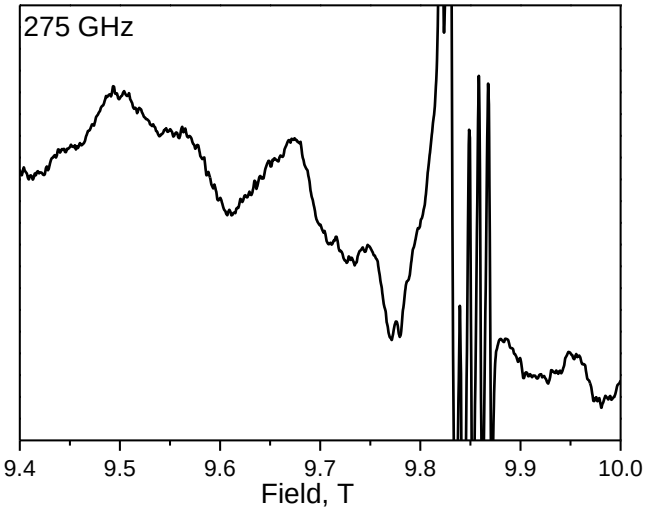

Figure 4.4. The cw EPR spectrum at 275.7 GHz and 10 K of the RFQ sample of pre-reduced T1D SLAC reacted with oxygen for 8 ms. Enzyme and oxygen concentration are 500 μM and 650 μM, respectively, both in 100 mM sodium phosphate buffer, pH 6.8. EPR measurements: modulation amplitude 2.8 mT and microwave power 2 μW.

Analysis of the EPR spectra

The quantitative analysis of the EPR spectra at 9.5, 94, and 275 GHz of the intermediate is based on the assumption that the spectra derive from a biradical, which consists of a Cu (II) (S = 1/2) in interaction with a tyrosyl radical (S = 1/2). We consider the following spin Hamiltonian

$$H = \beta_e \vec{S}^{Cu} \cdot \vec{\vec{g}}^{Cu} \cdot \vec{B} + \beta_e \vec{S}^{Tyr} \cdot \vec{\vec{g}}^{Tyr} \cdot \vec{B} + \vec{S}^{Cu} \cdot \vec{\vec{A}}^{Cu} \cdot \vec{I}^{Cu} + \vec{S}^{Cu} \cdot \vec{\vec{D}} \cdot \vec{S}^{Tyr} - J\vec{S}^{Cu} \cdot \vec{S}^{Tyr}$$

where β_e is the Bohr magneton, $\vec{S}^{Cu}$ and $\vec{S}^{Tyr}$ are the electron spin angular momentum operators, $\vec{\vec{g}}^{Cu}$ and $\vec{\vec{g}}^{Tyr}$ are the g-tensors of the copper and the radical center, $\vec{B}$ is the external magnetic field, $\vec{\vec{A}}^{Cu}$ and $\vec{I}^{Cu}$ are the hyperfine tensor and the nuclear spin angular momentum operator of copper, respectively, $\vec{\vec{D}}$ is the dipolar interaction tensor and J is the isotropic exchange coupling constant. A positive J corresponds to ferromagnetic coupling, i.e., a triplet ground state. The first two terms (Zeeman terms) in the spin Hamiltonian describe the interaction of the electron spins with the external magnetic field. The last two terms (the dipolar and exchange terms) describe the interactions between the two spins. We have not taken into account the hyperfine interaction of the α- and β-hydrogens of the tyrosyl radical. The spin Hamiltonian contains many parameters. To see whether this spin Hamiltonian provides a proper description of the EPR spectra of the intermediate and to obtain reliable values of the interaction parameters, we have to consider the EPR spectra at the three microwave frequencies in tandem.

At X-band, the hyperfine interaction of the electron spin with the copper nuclear spin and the interactions between the spins largely determine the spectrum. At higher microwave frequencies and magnetic fields, the contribution of the field-dependent terms of the spin Hamiltonian (the Zeeman terms) increases relative to that of the field-independent terms, which makes the 94 and 275 GHz spectra easier to interpret. The spectra of the RFQ sample of T1D SLAC at these microwave frequencies show less structure than the X-band spectrum. At these high frequencies, the hyperfine interactions are not resolved and only contribute to the linewidth.

The spin Hamiltonian parameters that are found to best reproduce the experimental spectra at 9.5, 94 and 275 GHz are listed in table 4.1.

Table 4.1. The spin Hamiltonian parameters that are found to best reproduce the experimental spectra of the freeze-quench samples of T1D SLAC at 9.5, 94 and 275 GHz. The *A*-, *J*- and *D* -value(s) are given in MHz. The Euler angles relate the orientation of the dipolar coupling tensor to the *g* principal axes of Cu and Tyr, which are assumed to be parallel. The standard deviations are estimated from the sensitivity of the simulated spectra to the variation of the parameters.

Parameters	g_x	g_y	g_z	A_x	A_y	A_z
Cu	2.037±0.002	2.067±0.002	2.25±0.01	30±10	40±10	580±15
Tyrosyl	2.0021 ±0.0020	2.0043 ±0.0020	2.0080 ±0.0030			
	D_x	D_y	D_z	J		
	290 ± 10	290 ± 10	−580 ± 20	12000 ± 1000		
			α_{dipole}	β_{dipole}	γ_{dipole}	
			−90	−85	90	

The principal axes systems of the copper *g* and the *A* tensors are taken parallel and define the axes system *x*, *y*, *z*. The *g*-tensor of tyrosyl is assumed to be diagonal in this axes system. The *D*-tensor is taken axial, and the Euler angles α, β and γ define the orientation of the *D*-tensor in this axes system. The simulations were performed using the EasySpin[34] package based on MATLAB.

The simulated EPR spectra are shown in figure 4.5 together with the experimental spectra. We have included the half-field spectrum at X-band.

In order to provide insight into the simulations, figure 4.5 also contains the energy-level diagrams as a function of the magnetic field, and the EPR transitions as red lines. The level of red indicates the probability of the transitions. At the highest magnetic field, at 275 GHz, the weak-coupling limit is not reached. Even for the magnetic field along the *z*-direction, for which the difference in g values is largest, the condition $|J| \ll (|g^{Cu}-g^{Tyr}|)\beta_e B$ is not fulfilled. The difference in the g_z values of 0.242 in frequency units corresponds to about 30 GHz in a field of 9 T, which is less than three times the exchange interaction. Nevertheless, the diagram for the magnetic field parallel *z* at 275 GHz in figure 4.5 shows the pair of doublet transitions expected in the weak-coupling limit (cf. chapter 1). The doublets are centered at the resonance fields of the respective spins, at 8.75 for Cu and 9.81 T for the tyrosyl radical, but the outer lines have relatively low intensity. The corresponding lines become very weak for the magnetic field parallel *x* and *y*, for which the difference in g values of Cu and the tyrosyl radical is much smaller and the deviation from the weak-coupling limit larger.

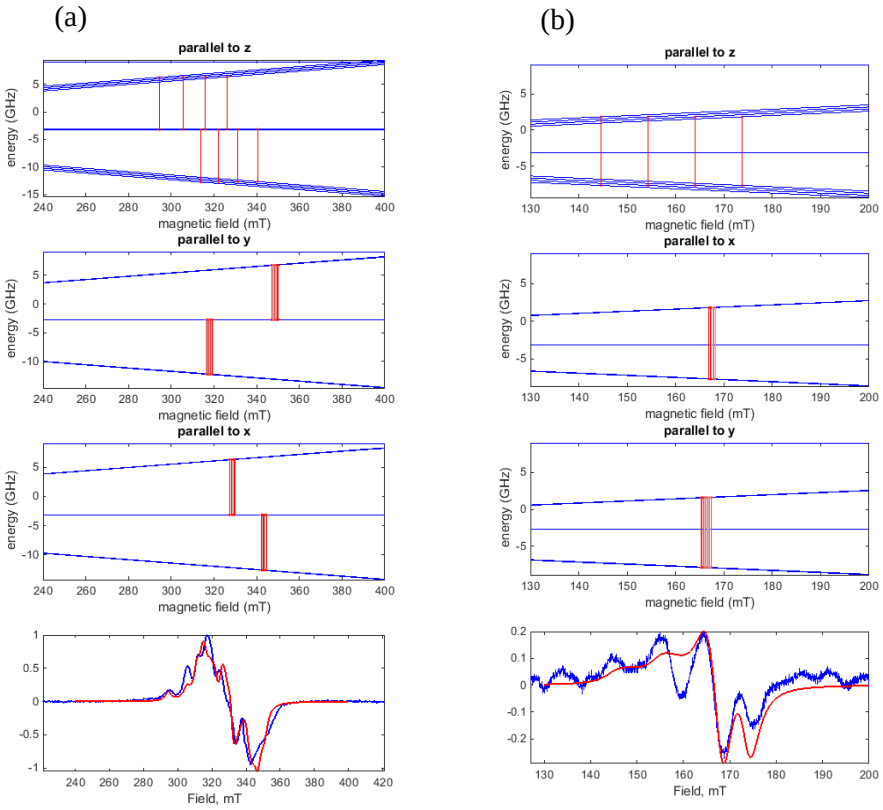

Figure 4.5. Comparison of the simulated and experimental EPR spectra of the T1D SLAC intermediate at 9.5 GHz (a,b), at 94.1 GHz (c) and 275.7 GHz (d). The spectra correspond to the reaction time of 8ms. The simulations are performed at the temperature at which the experimental spectra were recorded, (a) at 7K, (b) and (c) at 40 K, and (d) at 10 K. The spin Hamiltonian parameters used for the simulations are given in table 4.1. In the upper panels the energy levels as a function of magnetic field are presented for three orientations of the magnetic field, along the *x*, *y* and *z* direction. The EPR transitions are indicated, and the intensity of the lines refers to the corresponding transition probabilities. The lines shown in gray have low transition probabilities.

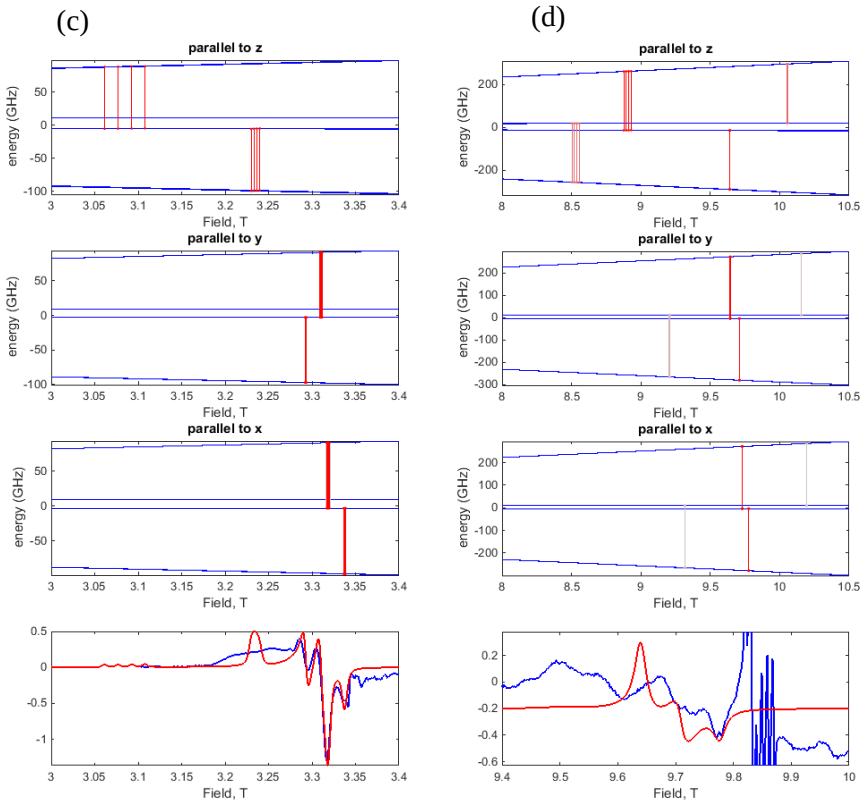

At 9.5 GHz, the difference in the g_z values of 0.242 in frequency units corresponds to about 1.1 GHz in a field of 320 mT. The strong-coupling limit, $|J| \gg (|g^{Cu}\text{-}g^{Tyr}|)\beta_e B$, holds. If the spins would not experience a dipolar interaction, the EPR spectrum would correspond to two transitions that coincide at the average resonance field of the two spins (cf. chapter 1), which would be at about 318.8 mT. In the presence of the dipolar interaction, they are split into two transitions. The same applies

for the magnetic field parallel to *x* and *y*. A further splitting is visible, which derives from the copper hyperfine coupling.

The EPR spectra at 9.5, 94 and 275 GHz depend on all spin Hamiltonian parameters, be it to a different extent, which forms the basis for their determination. The exchange interaction *J* of 12 GHz is obtained from the simulation of the EPR spectra at 94 and 275 GHz. The simulations were also performed with a *J* of −12 GHz, while dipolar interaction and other parameters were kept constant. The negative value of *J* yields a large signal around 10 T at 275 GHz (figure 4.6), which is not compatible with the experimental spectrum. Variation of the dipolar interaction and the g-values did not produce a simulation for $J < 0$ that fits the experimental spectrum. The high-field spectra also are most sensitive to the g_x and g_y values of copper and the *g* values of the tyrosyl radical. The latter principal values refer to the principal axes system of copper *g*-tensor. The low-field parts of the spectra at 94 and 275 GHz are not informative as the transitions for the magnetic field along the z direction are broadened due to copper g-strain. The simulation of the 94 GHz spectrum is consistent with the observation that the signal centered at 3.32 T loses intensity as the temperature is reduced from 40 to 15 K (figure 4.3). The two transitions that nearly coincide at this field both concern transitions between the upper levels. The principal values and the orientation of the dipolar interaction tensor are obtained from the simulation of the EPR spectra at 9.5 (g=2 region) and 94 GHz. The Euler angles in table 4.1 reveal that the dipolar axis (corresponding to the axiality of the D tensor) virtually coincides with the direction of the copper g_y axis. The copper hyperfine tensor and the g_z value of copper are obtained from the simulation of the g = 4 region (140 to 180 mT) and the

g = 2 region (290 to 340 mT) of the spectrum at 9.5 GHz (see figure 4.5a and b). The copper hyperfine interaction largely determines the structure of the EPR spectrum at this microwave frequency.

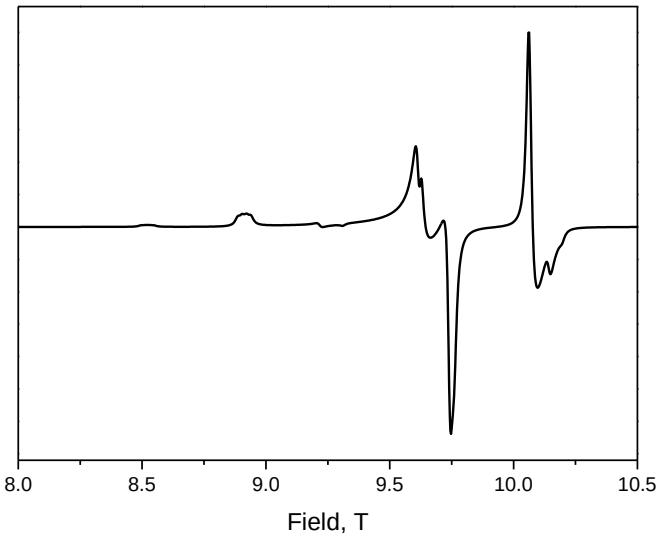

Figure 4.6. The simulated EPR spectrum at 10 K and 275.7 GHz for the J = − 12 GHz. The other parameters are as given in table 4.1.

4.3.2 Reoxidation of T1D Y108F SLAC

The X-band EPR spectra at 40 K of freeze-quench samples of pre-reduced Y108F T1D SLAC reacted with oxygen for different times between 8 milliseconds and 40 seconds are presented in figure 4.7. These spectra were recorded with a modulation amplitude of 0.5 mT. No further (hyperfine) structure was resolved when the modulation amplitude was reduced to 0.2 mT.

All the spectra are normalized according to the signal of Mn(II) at 361 mT as an internal standard. Some of the Mn(II) signals are marked with an asterisk, while others are hidden in the signal from the enzyme. The spectra in figure 4.7 extend from 265 to 365 mT. The low-field hyperfine band at 272 mT points to a T2 Cu signal. On top of the Cu signal, there is a narrow signal at g ≈ 2 (centered at 338.5 mT) with a linewidth of 2.1 mT.

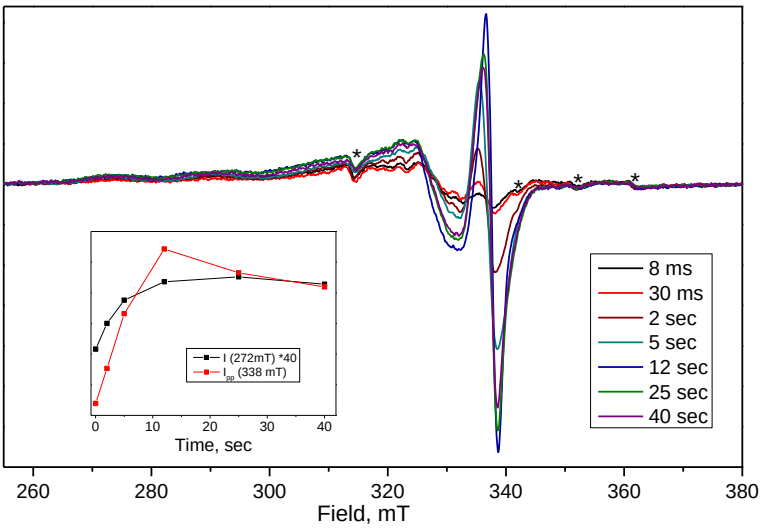

Figure 4.7. The cw X-band EPR spectra of freeze-quench samples of reduced Y108F T1D SLAC reacted with oxygen for different times. The inset shows the change in the intensity of the 270 mT signal (×40) and the peak-to-peak intensity of the narrow signal centered at 337.5 mT. Enzyme and oxygen concentration are 450 μM and 650 μM, respectively, both in 100 mM sodium phosphate buffer, pH 6.8. EPR measurements: microwave frequency 9.5 GHz, T = 40 K, microwave power 0.16 mW and modulation amplitude 0.5 mT. The signals marked with an asterisk originate from Mn(II).

The change of the intensity of 272 mT signal and of the signal centered at 338.5 mT is presented in the inset of figure 4.7. Both signals grow with the reaction time up till 12 s, be it not at the same rate.

Figure 4.8 shows difference spectra obtained after normalization at 272 mT of some of the spectra in figure 4.7. Subtraction removes the T2 Cu signal and the difference spectra show more clearly the change in time of the additional paramagnetic signal, which largely concerns the narrow, radical-like signal.

Spin quantification indicates that the ratio of the narrow signal to the copper signal for the sample with reaction time of 12 seconds is about 0.15.

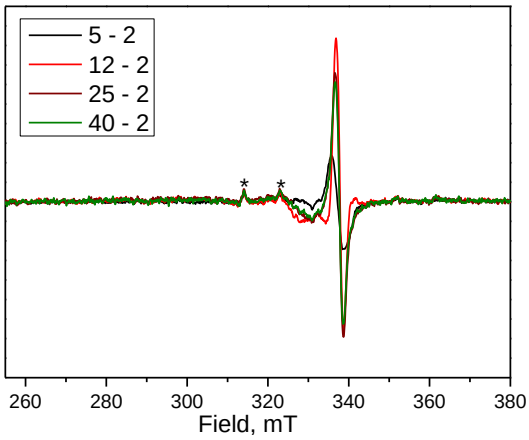

Figure 4.8. The difference X-band EPR spectra of the freeze-quench samples of Y108F T1D SLAC derived from subtraction of the spectrum with the reaction time of 2 seconds from the spectra corresponding to the reaction times of 5, 12, 25 and 40 seconds, after normalizing at 272 mT. The signals marked with an asterisk originate from Mn(II).

Figure 4.9 shows an overlay of the EPR spectrum of the freeze-quench sample for the reaction time of 40 seconds, the longest time for which the reaction was followed, and that of the resting form of the enzyme (Y108F T1D SLAC). The spectra are normalized according to the signal of Mn(II) at 361 mT. The copper signals in both spectra show a similar field dependence, and comparison of the intensities of the signals shows that the T2 Cu is not completely reoxidized after 40 seconds.

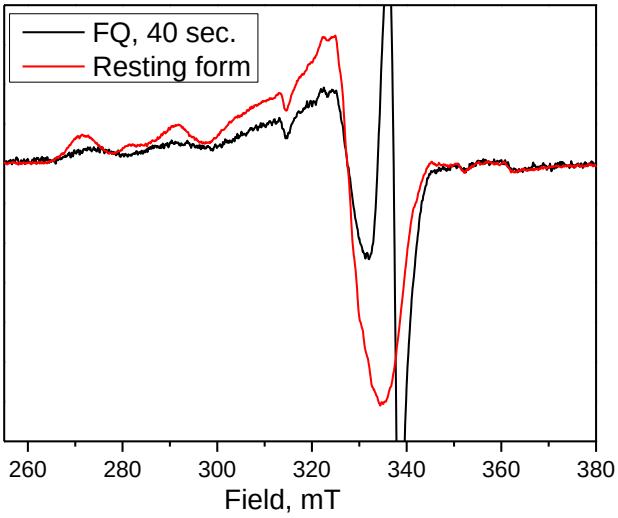

Figure 4.9. The overlay of the EPR spectrum of the freeze-quench sample for the reaction time of 40 seconds, and that of the resting form of the enzyme (Y108F T1D SLAC). The spectra are normalized according to the signal of Mn(II) at 361 mT. EPR measurements: microwave frequency 9.5 GHz, T = 40 K, microwave power 0.16 mW and modulation amplitude 0.5 mT.

To get further insight into the EPR spectra of the freeze-quench samples of fully reduced T1D Y108F SLAC reacted with oxygen, the spectra of

the samples reacted for 5 and 25 seconds were also measured at 94 GHz. The EPR spectra for both samples were the same. The spectrum of the 25 seconds sample is presented in figure 4.10. This spectrum consists of a broad band, which extends from 3.25 to 3.33 T, and a narrow signal with a linewidth of 5.5 mT at about 3.36 T. This signal overlaps with the six lines of Mn(II), which show up between 3.33 and 3.38 T.

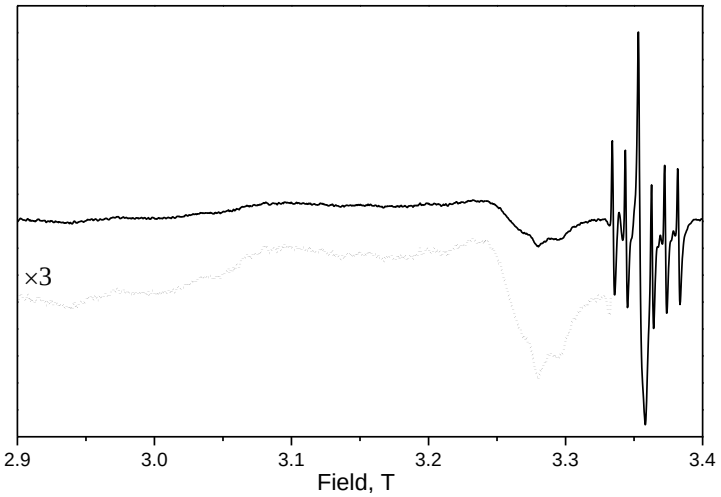

Figure 4.10. The cw 94.1 GHz EPR spectrum of the freeze-quench sample of pre-reduced T1D Y108F reacted with oxygen for 25 seconds. The enlarged (×3) copper signal is shown as dotted line. Enzyme and oxygen concentration are 450 μM and 650 μM, respectively, both in 100 mM sodium phosphate buffer, pH 6.8. EPR measurements: temperature 40 K, modulation amplitude 1.2 mT and microwave power 50 μW.

Analysis of the EPR spectra

Comparison of the EPR spectra of the freeze-quench samples of Y108F T1D at 9.5 and 94 GHz shows that they are the sum of a copper signal and a radical signal. To obtain the spectrum of the radical at 9.5 GHz, the spectrum of the resting form of Y108F T1D was subtracted from the spectrum of the freeze-quench sample reacted for 25 seconds after normalization at 272 mT, thus removing the T2 Cu contribution to the spectrum. The resultant spectrum of the radical is presented in figure 4.11a, solid line. At 94 GHz, the copper and radical signals are nicely separated. The spectrum of the radical signal is obtained after subtraction of the Mn(II) signals, which is imperfect as is clear from figure 4.11b, solid line.

To simulate the radical spectra at 9.5 and 94 GHz, only the Zeeman term of the spin Hamiltonian is considered.

$$H = \beta_e \vec{S} \cdot \vec{\vec{g}} \cdot \vec{B}$$

A proper description of the spectra at both microwave frequencies is obtained in terms of a radical with g-values of 2.0010, 2.00034 and 2.0043 (figure 4.11, dashed lines).

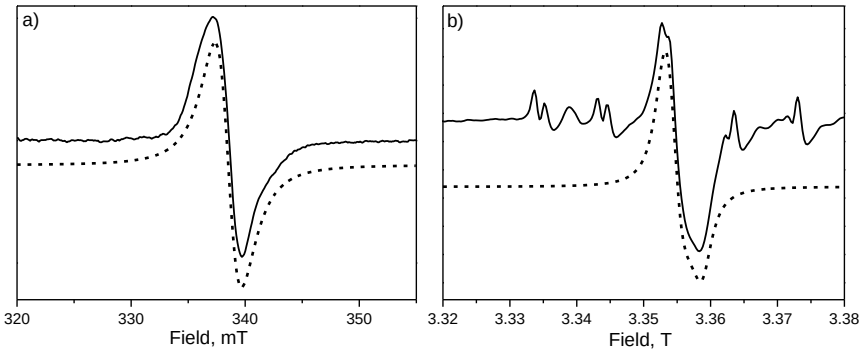

Figure 4.11. Comparison of the experimental (solid lines) and simulated spectra (dashed lines) at (a) 9.5 and (b) 94 GHz of the radical part of the EPR spectra of reduced Y108F T1D SLAC reacted with oxygen for 25 seconds. The way the experimental spectra are obtained is outlined in the text. The simulated spectra correspond to a radical with g-values of 2.0010, 2.00034 and 2.0043, and a linewidth of 2.3 and 2.1 mT for 9.5 and 94 GHz spectra, respectively. The simulations are performed with the EasySpin[34] package based on MATLAB.

4.4 Discussion

We have investigated the early stage of the reoxidation of T1D SLAC with molecular oxygen using multi-frequency EPR spectroscopy in combination with the RFQ technique. An intermediate has been trapped on the time scale of milliseconds and characterized based on the analysis of EPR spectra at 9, 94 and 275 GHz. The X-band EPR spectrum of the intermediate does not change for reaction times between 8 and 105 ms (figure 4. 2). This spectrum is essentially identical to that obtained previously from the difference of the measured spectra corresponding to different reaction times during the decay of the intermediate on the time scale of minutes[7], as shown in figure 4.12. This identity concerns both

the g = 2 and the g = 4 region of the spectrum. The only difference is in the signal to noise ratio for the latter part of the spectrum, which is lower for the spectrum of the RFQ sample on the time scale of milliseconds. Both the concentration and the amount of sample in the EPR tube were less for the RFQ sample than for the manually mixed samples studied at the time scale of minutes to hours. The identity of the EPR spectra of the intermediates from milliseconds to hours reveals that only one paramagnetic intermediate, a biradical, shows up during the reoxidation of fully reduced T1D SLAC by molecular oxygen.

The second order rate constant of $1.7 \pm 0.3 \times 10^5\ M^{-1}s^{-1}$ for the single turnover of T1D SLAC at pH 6.8 obtained in this study is in good agreement with that of $2.3 \times 10^5\ M^{-1}s^{-1}$ at pH 6 obtained by transient fluorescence spectroscopy[9] (see figure S4 of ref. 9), considering that the reoxidation of laccases is a pH-dependent process[35]. The rate constant obtained from the RFQ/EPR experiments is also in excellent agreement with the value of $1.8 \pm 0.08 \times 10^5\ M^{-1}s^{-1}$ obtained by transient absorbance spectroscopy, following the growing of the 420 nm band[7]. This result strongly supports the conclusion that the EPR and optical signatures derive from the formation of the same intermediate, as observed previously for the decay of the intermediate.

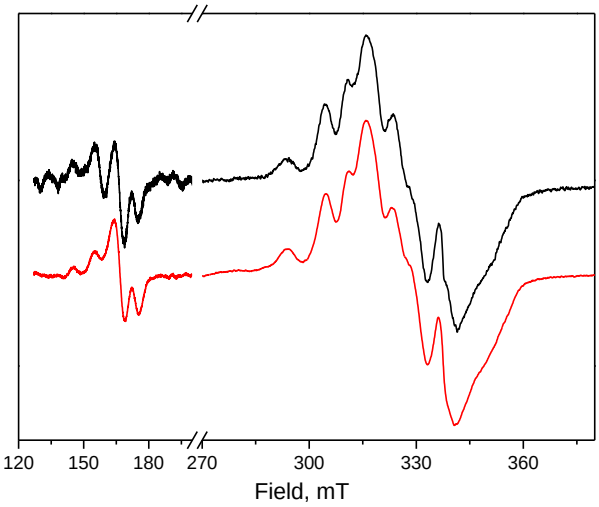

Figure 4. 12. The cw X-band EPR spectra of the intermediate as measured for the 8 ms-RFQ sample of T1D SLAC reacted with oxygen (black line) and derived from the difference of the spectra corresponding to different reaction times during the decay of the intermediate on the time scale of minutes (red line). Enzyme concentration is 500 μM and 700 μM for the RFQ sample and manually mixed samples, respectively, in 100 mM sodium phosphate buffer, pH 6.8. EPR measurements: microwave frequency 9.5 GHz, T = 40 K, microwave power 0.16 mW and modulation amplitude 0.5 mT for the g = 2 signal, and T = 7 K, microwave power 20 mW and modulation amplitude 1.5 mT for the g = 4 signal. The vertical scales for the g = 2 and g = 4 signals are different.

In figure 4.13 we summarize the 9.5 GHz EPR spectra that characterize the various stages of the reoxidation cycle of T1D SLAC: of the resting form of the protein as purified (the upper spectrum), of the reduced form, of the intermediate, during formation (105 ms) and decay (2 minutes), and of the reoxidized form. The EPR spectrum of the resting form of T1D SLAC, as described in chapter 1, shows a signal characteristic for

T2 Cu. Lines at 272, at 293, and at 314 mT indicate the copper hyperfine interaction, with the fourth hyperfine line hidden in the g_x, g_y region. In addition, the spectrum nicely shows a small hyperfine structure around 328 mT, which derives from the interaction of the electron spin with the nitrogen nuclei of the copper-coordinating histidines. When the enzyme is reduced, there is no EPR signal, because of the d^{10} electron configuration of Cu (I), except for a small signal (< 10%) of unreduced copper.

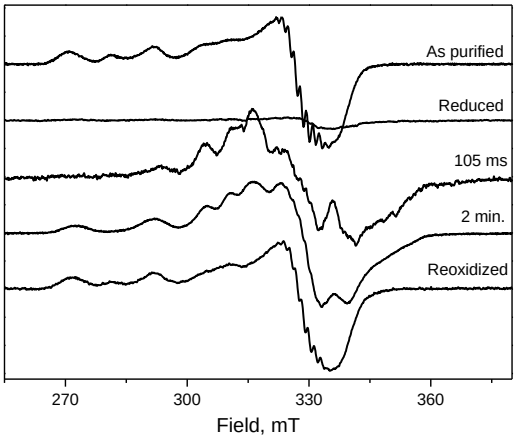

Figure 4. 13. The cw X-band EPR spectra of T1D SLAC of the resting form (as purified), the reduced form and the biradical intermediate, during the formation (100 ms) and the decay (2 minutes) and the reoxidized resting form, as observed after 5 hrs under aerobic condition. EPR measurements: microwave frequency 9.49 GHz, T = 40 K, microwave power 0.16 mW and modulation amplitude 0.5 mT.

Upon mixing of the reduced enzyme with oxygen, the intermediate quickly starts to form and is observed at the shortest observation time, 8 ms, of our RFQ setup. The intermediate spectrum, e.g. the spectrum of

the 105 ms-RFQ sample, is clearly different from the spectrum of the resting form. It shows more structure, contains an additional broad signal around 350 mT and lacks the low-field hyperfine signal of T2 Cu at 272 mT. The 272 mT-hyperfine signal of Cu reappears for the samples with the reaction time of minutes, which implies the decay of the intermediate to the resting form of the enzyme. The spectrum of the sample at two minutes is a superposition of the spectra of the intermediate and of the resting form of the enzyme. The spectrum of the reoxidized form is essentially the same as that of the protein as purified.

The spin quantification shows that more than one unpaired electron per enzyme molecule contributes to the EPR spectra in figure 4.2, e.g. 1.9 for the sample at 105 ms. Previously, based on the splitting of the half-field signal into four equidistant lines and the similarity of this signal to those for spin-labeled copper compounds, it was concluded that one of the spins resides on a Cu in the TNC[1]. Based on the absorbance signature (420 nm band) and the estimated spin-spin distance of 5 Å, it was proposed that the second spin resides on an amino-acid-derived radical, most probably tyrosine 108 (Y108)[7].

The analysis of our multi-frequency EPR spectra for the reoxidation of the T1D SLAC on the time scale of milliseconds strongly supports the previous proposal. The results unambiguously prove that the EPR spectrum of the intermediate derives from the biradical consisting of the T2 Cu and the tyrosyl (Y108) radical, coupled by an exchange interaction of 12 GHz and a dipolar interaction of [290 290 −580] MHz. The EPR spectra at 9.5, 94 and 275 GHz have consistently been simulated with one set of spin-Hamiltonian parameters.

For copper, the g_z value (2.25) and the *A* tensor (30 40 580) obtained from the simulation of the 9.5 GHz spectrum and the value of g_x (2.037) and of g_y (2.067) obtained from the simulation of the 94 and 275 GHz spectra are consistent with values reported for T2 Cu[1-3]. For the radical, the *g* values (2.0021 2.0043 2.0080) are compatible with values reported for a tyrosine radical[10]. The largest *g*-value of tyrosyl radicals is particularly sensitive to the structure and the environment of the radical[10].

The dipolar interaction fulfills the following equation:

$$D = -\frac{\mu_0 \beta_e^2}{8\hbar\pi^2} \frac{g_{Cu} g_{Tyr}}{r^3} (3\cos^2\theta - 1) \qquad (1)$$

where g^{Cu} and g^{Tyr} are the *g*-values for T2 Cu and Y108, respectively, r is the interspin distance, and θ is the angle between the line connecting the unpaired electrons and the direction of the external magnetic field.

The dipolar interaction of [290 290 −580] MHz obtained from the EPR spectra at 9.5, 94 and 275 GHz yields, according to eq. 1, an interspin distance of 5.7 ± 0.1 Å between the T2 Cu and the Y108 radical. This value is in line with the distance previously estimated from the ratio of the intensities of the g = 4 and g = 2 signals for the biradical intermediate detected on the time scale of minutes[7]. The crystal structure of SLAC (PDB: 3CG8) shows that the oxygen of Y108 is located 4.5 Å away from T2 Cu, which is in excellent agreement with the obtained distance of 5.7 Å. At this distance the point-dipole approximation is valid, and the calculated distance corresponds to the distance between the centers of the spin-density distributions at the copper and the tyrosine. For tyrosine about 75% of the spin density is distributed over the aromatic ring[36]. The

distance between the T2 Cu and the carbon of aromatic ring that is bonded to oxygen of Y108 is 5.6 Å, according to the 3D structure of SLAC. This corroborates the assignment of the radical as Y108.

The positive sign of the exchange interaction obtained in our study indicates the ferromagnetic coupling between the unpaired electrons of T2 Cu and the Y108 radical for SLAC, resulting in a triplet (S = 1) ground state. The coupling between copper and a tyrosyl radical can also be antiferromagnetic, resulting in a singlet (S = 0) ground state, as reported for galactose oxidase[16,17].

In view of the interspin distance of 5.7 Å, the magnitude of 12±0.5 GHz of the exchange interaction is within the range reported for similar systems. The magnitude of the exchange interaction depends on the overlap of the wave functions of the two electrons and consequently on the interspin distance. The value of *J* for the interaction between a metal ion and an organic radical (a nitroxide or an amino-acid-based radical) with an interspin distance of 4.6 – 10 Å has been found to vary dramatically from a few MHz to thousands of GHz[25]. For instance, the value of *J* varies between 300 MHz and 4800 GHz for a Cu(II) and a nitroxide with the interspin distance of 4.6 – 8 Å in spin-labeled copper complexes[36,37]. An interspin distance of 7.7 – 8 Å between a tyrosyl radical and a tetrahedral manganese cluster in acetate-inhibited photosystem II and between a tyrosyl radical and a diferric cluster in class I ribonucleotide reductase leads to an exchange interaction of 840[19] MHz and 150[18] MHz, respectively. In other words, the exchange interaction is a sensitive measure of the electronic structure, but cannot simply be translated into an interspin distance.

For Y108F T1D SLAC, in which tyrosine 108 has been replaced by phenylalanine by site-directed mutagenesis, there is no sign of a biradical intermediate on the time scale of milliseconds to seconds (Figure 4. 5). This reinforces our conclusion as regards the crucial role of tyrosine 108 in the reaction of T1D SLAC with molecular oxygen. The EPR spectra consist of signals of T2 Cu and of a radical, which increase at different rates when the reaction goes on from milliseconds to seconds. Combination of the spectra at 9.5 and 94 GHz shows no interaction of the spins. Although the signal of the radical is small, it grows and decays during the reaction, which implies that the radical is involved in the reoxidation process in one way or another. The rate of formation of the paramagnetic species also differs from that for T1D SLAC. Based on spin quantification, the signal observed at the earliest time point (8 ms) corresponds to less than 10% of total protein for Y108F T1D SLAC and about 100 % for T1D SLAC. The best fit to the 9 and 94 GHz spectra of the radical was obtained for *g*-values of 2.0010, 2.0034 and 2.0043. As regards the assignment of the radical, the small *g*-anisotropy excludes an oxygen- or sulfur-based radical such as a tyrosyl or a cysteinyl radical[10,11]. Glycyl radicals are unstable in the presence of oxygen and are restricted to anaerobic enzymatic reaction[10]. Moreover, a glycyl radical typically shows a doublet in the 9 GHz EPR spectrum[38], which is not observed for the T1D Y108F SLAC samples. Tryptophanyl radicals commonly show small g-anisotropy and no appreciable hyperfine structure at 9 GHz[10,11]. We tentatively assign the radical observed during the reoxidation of T1D Y108F SLAC to a tryptophanyl radical. We cannot exclude that the radical does not participate in the oxygen reduction as its amount is quite small (> 15%).

Interestingly, for both mutants of SLAC (T1D and Y108F T1D), an amino acid from the enzyme participates in the reduction of oxygen. As oxygen reduction needs four electrons, and only three electrons are available from the TNC in the absence of T1 Cu (T1D), the enzyme finds another source of an electron to prevent the formation of oxygen-reactive species and consequently protect the enzyme from oxidative degradation. In this respect, the present study reveals the prime role of Y108 for SLAC. Remarkably, the Y108 is conserved between the SLAC-like type B 2dMCO's and also 6-domain human ceruloplasmin[9,39]. The protective role of tyrosine and tryptophan has been reported for many enzymes, especially those that form high-potential intermediates[40]. If these residues are located in an appropriate place, they can protect the enzyme by rapid reduction of such intermediates or prevent the formation of harmful species such as oxygen-reactive species by providing an electron. Interestingly, 66% of the O_2-reactive oxidoreductases have tyrosine frequencies above the database average of the Enzyme Data Bank of the Swiss Institute of Bioinformatics and 81% have above-average tryptophan frequencies[40]. Our observation for the T1D SLAC is in line with the proposed protective role of tyrosine and tryptophan as an endogenous reducing agent, which effectively protects enzymes from oxidative degradation[13,40].

4.5 Conclusion

We used multi-frequency EPR in combination with the rapid freeze-quench technique to trap and characterize intermediates formed during the reaction of fully reduced T1D and T1D Y108F SLAC with oxygen on the time scale of milliseconds. The X-band EPR spectra of the T1D SLAC intermediate with the reaction time of milliseconds are essentially identical to those previously derived from the difference of the spectra corresponding to different reaction time during the decay of the intermediate on the time scale of minutes[7]. The identity of the EPR spectra of the intermediates from milliseconds to hours reveals that only one paramagnetic intermediate shows up during the reoxidation of fully reduced T1D SLAC by molecular oxygen. The combined analysis of EPR data at 9, 94 and 275 GHz of RFQ samples of T1D SLAC unambiguously indicates that the intermediate consists of the T2 Cu and the tyrosyl 108 radical. For Y108F T1D SLAC, we observed no sign of a biradical intermediate during the reoxidation process on the time scale of milliseconds to seconds. This reinforces our conclusion as regards the crucial role of tyrosine 108 in the reaction of T1D SLAC with molecular oxygen. For Y108F T1D SLAC, we observed an intermediate with a small contribution from a radical, which is tentatively assigned to a tryptophanyl radical based on its small g-anisotropy. As reduction of oxygen to water needs four electrons, and the coppers in T1D mutants provide only three electrons, the enzyme finds another source of an electron to complete the reaction and prevent the formation of oxygen-reactive species. The protective role of tyrosine and tryptophan is likely an evolutionary adaptation to protect the enzyme from oxidative degradation.

In view of our observations for T1D SLAC, the possible role of tyrosine 108 during the reoxidation of fully reduced wild-type SLAC with O_2 is worth to be investigated. This is the subject of the chapter 5. Mechanistic implications will be discussed in chapter 6.

References

(1) Solomon, E. I.; Augustine, A. J.; Yoon, J. O_2 Reduction to H_2O by the Multicopper Oxidases. *Dalton Trans.* **2008**, 30, 3921–3932.

(2) Solomon, E. I.; Chen, P.; Metz, M.; Lee, S.-K.; Palmer, A. E. Oxygen Binding, Activation, and Reduction to Water by Copper Proteins. *Angew. Chemie Int. Ed.* **2001**, *40* (24), 4570–4590.

(3) Jones, S. M.; Solomon, E. I. Electron Transfer and Reaction Mechanism of Laccases. *Cell. Mol. Life Sci.* **2015**, *72* (5), 869–883.

(4) Wherland, S.; Farver, O.; Pecht, I. Multicopper Oxidases: Intramolecular Electron Transfer and O_2 Reduction. *J. Biol. Inorg. Chem.* **2014**, *19*, 541–554.

(5) Komori, H.; Higuchi, Y.; Ions, F. C. Structural Insights into the O_2 Reduction Mechanism of Multicopper Oxidase. *J. Biochem.* **2015**, *158* (4), 293–298.

(6) Machczynski, M. C.; Vijgenboom, E.; Samyn, B.; Canters, G. W. Characterization of SLAC: A Small Laccase from Streptomyces Coelicolor with Unprecedented Activity. *Protein Sci.* **2004**, *13* (9), 2388–2397.

(7) Tepper, A. W. J. W.; Milikisyants, S.; Sottini, S.; Vijgenboom, E.; Groenen, E. J. J.; Canters, G. W. Identification of a Radical Intermediate in the Enzymatic Reduction of Oxygen by a Small Laccase. *J. Am. Chem. Soc.* **2009**, *131* (33), 11680–11682.

(8) Skálová, T.; Dohnálek, J.; Østergaard, L. H.; Østergaard, P. R.; Kolenko, P.; Dušková, J.; Štěpánková, A.; Hašek, J. The Structure of the Small Laccase from Streptomyces Coelicolor Reveals a Link between Laccases and Nitrite Reductases. *J. Mol. Biol.* **2009**, *385* (4), 1165–1178.

(9) Gupta, A.; Nederlof, I.; Sottini, S.; Tepper, A. W. J. W.; Groenen, E. J. J.; Thomassen, E. A. J.; Canters, G. W. Involvement of Tyr108 in the Enzyme Mechanism of the Small Laccase from

Streptomyces Coelicolor. *J. Am. Chem. Soc.* **2012**, *134* (44), 18213–18216.

(10) Jeschke, G. EPR Techniques for Studying Radical Enzymes. *Biochim. Biophys. Acta - Bioenerg.* **2005**, *1707*, 91–102.

(11) Stubbe, J.; Van der Donk, W. A. Protein Radicals in Enzyme Catalysis. *Chem. Rev.* **1998**, *98* (2), 705–762.

(12) Svistunenko, D. A.; Cooper, C. E. A New Method of Identifying the Site of Tyrosyl Radicals in Proteins. *Biophys. J.* **2004**, *87* (1), 582–595.

(13) Dumarieh, R.; D'Antonio, J.; Deliz-Liang, A.; Smirnova, T.; Svistunenko, D. A.; Ghiladi, R. A. Tyrosyl Radicals in Dehaloperoxidase. *J. Biol. Chem.* **2013**, *288* (46), 33470–33482.

(14) Hoganson, C. W.; Tommos, C. The Function and Characteristics of Tyrosyl Radical Cofactors. *Biochim. Biophys. Acta - Bioenerg.* **2004**, *1655* (1–3), 116–122.

(15) Rogers, M. Copper-Tyrosyl Radical Enzymes. *Curr. Opin. Chem. Biol.* **2003**, *7* (2), 189–196.

(16) Babcock, G. T.; El-Deeb, M. K.; Sandusky, P. O.; Whittaker, M. M.; Whittaker, J. W. Electron Paramagnetic Resonance and Electron Nuclear Double Resonance Spectroscopies of the Radical Site in Galactose Oxidase and of Thioether-Substituted Phenol Model Compounds. *J. Am. Chem. Soc.* **1992**, *114* (10), 3727–3734.

(17) Müller, J.; Weyhermüller, T.; Bill, E.; Hildebrandt, P.; Ould-Moussa, L.; Glaser, T.; Wieghardt, K. Why Does the Active Form of Galactose Oxidase Possess a Diamagnetic Ground State? *Angew. Chemie Int. Ed.* **1998**, *37* (5), 616–619.

(18) Hirsh, D. J.; Beck, W. F.; Lynch, J. B.; Que, L.; Brudvig, G. W. Using Saturation-Recovery EPR to Measure Exchange Couplings in Proteins: Application to Ribonucleotide Reductase. *J. Am. Chem. Soc.* **1992**, *114* (19), 7475–7481.

(19) Lakshmi, K. V; Eaton, S. S.; Eaton, G. R.; Frank, H. A.; Brudvig,

G. W. Analysis of Dipolar and Exchange Interactions between Manganese and Tyrosine Z in the S 2 Y. **1998**, *5647* (98), 8327–8335.

(20) Lassmann, G.; Odenwaller, R.; Curtis, J. F.; DeGray, J. A.; Mason, R. P.; Marnett, L. J.; Eling, T. E. Electron Spin Resonance Investigation of Tyrosyl Radicals of Prostaglandin H Synthase. Relation to Enzyme Catalysis. *J. Biol. Chem.* **1991**, *266* (30), 20045–20055.

(21) Tsai, A. L.; Wu, G.; Palmer, G.; Bambai, B.; Koehn, J. A.; Marshall, P. J.; Kulmacz, R. J. Rapid Kinetics of Tyrosyl Radical Formation and Heme Redox State Changes in Prostaglandin H Synthase-1 and -2. *J. Biol. Chem.* **1999**, *274* (31), 21695–21700.

(22) MacMillan, F.; Kannt, A.; Behr, J.; Prisner, T.; Michel, H. Direct Evidence for a Tyrosine Radical in the Reaction of Cytochrome c Oxidase with Hydrogen Peroxide. *Biochemistry* **1999**, *38* (29), 9179–9184.

(23) Yu, M. A.; Egawa, T.; Shinzawa-Itoh, K.; Yoshikawa, S.; Guallar, V.; Yeh, S.-R.; Rousseau, D. L.; Gerfen, G. J. Two Tyrosyl Radicals Stabilize High Oxidation States in Cytochrome C Oxidase for Efficient Energy Conservation and Proton Translocation. *J. Am. Chem. Soc.* **2012**, *134* (10), 4753–4761.

(24) Yu, Y.; Mukherjee, A.; Nilges, M. J.; Hosseinzadeh, P.; Miner, K. D.; Lu, Y. Direct EPR Observation of a Tyrosyl Radical in a Functional Oxidase Model in Myoglobin during Both H_2O_2 and O_2 Reactions. *J. Am. Chem. Soc.* **2014**, *136* (4), 1174–1177.

(25) Manzerova, J.; Krymov, V.; Gerfen, G. J. Investigating the Intermediates in the Reaction of Ribonucleoside Triphosphate Reductase from Lactobacillus Leichmannii: An Application of HF EPR-RFQ Technology. *J. Magn. Reson.* **2011**, *213* (1), 32–45.

(26) Kuchenreuther, J. M.; Myers, W. K.; Stich, T. A.; George, S. J.; Nejatyjahromy, Y.; Swartz, J. R.; Britt, R. D. A Radical Intermediate in Tyrosine Scission to the CO and CN- Ligands of

FeFe Hydrogenase. *Science* **2013**, *342* (6157), 472–475.

(27) Suarez, J.; Ranguelova, K.; Jarzecki, A. A.; Manzerova, J.; Krymov, V.; Zhao, X.; Yu, S.; Metlitsky, L.; Gerfen, G. J.; Magliozzo, R. S. An Oxyferrous Heme/protein-Based Radical Intermediate Is Catalytically Competent in the Catalase Reaction of Mycobacterium Tuberculosis Catalase-Peroxidase (KatG). *J. Biol. Chem.* **2009**, *284* (11), 7017–7029.

(28) Rittle, J.; Green, M. T. Cytochrome P450 Compound I: Capture, Characterisation, and C--H Bond Activation Kinetics. *Science.* **2010**, *330*, 933–937.

(29) Grove, T. L.; Livada, J.; Schwalm, E. L.; Green, M. T.; Booker, S. J.; Silakov, A. A Substrate Radical Intermediate in Catalysis by the Antibiotic Resistance Protein Cfr. *Nat. Chem. Biol.* **2013**, *9* (7), 422–427.

(30) De Vries, S.; Dörner, K.; Strampraad, M. J. F.; Friedrich, T. Electron Tunneling Rates in Respiratory Complex I Are Tuned for Efficient Energy Conversion. *Angew. Chemie Int. Ed.* **2015**, *54* (9), 2844–2848.

(31) Blok, H.; Disselhorst, J. A. J. M.; Orlinskii, S. B.; Schmidt, J. A Continuous-Wave and Pulsed Electron Spin Resonance Spectrometer Operating at 275 GHz. *J. Magn. Reson.* **2004**, *166* (1), 92–99.

(32) Mathies, G.; Blok, H.; Disselhorst, J. A. J. M.; Gast, P.; Van der Meer, H.; Miedema, D. M.; Almeida, R. M.; Moura, J. J. G.; Hagen, W. R.; Groenen, E. J. J. Continuous-Wave EPR at 275 GHz: Application to High-Spin Fe3+ Systems. *J. Magn. Reson.* **2011**, *210* (1), 126–132.

(33) Nami, F.; Gast, P.; Groenen, E. J. J. Rapid Freeze-Quench EPR Spectroscopy : Improved Collection of Frozen Particles. *Appl. Magn. Reson.* **2016**, 1–7.

(34) Stoll, S.; Schweiger, A. EasySpin, a Comprehensive Software Package for Spectral Simulation and Analysis in EPR. *J. Magn. Reson.* **2006**, *178* (1), 42–55.

(35) Shin, W.; Sundaram, U. M.; Cole, J. L.; Zhang, H. H.; Hedman, B.; Hodgson, K. O.; Solomon, E. I. Chemical and Spectroscopic Definition of the Peroxide-Level Intermediate in the Multicopper Oxidases: Relevance to the Catalytic Mechanism of Dioxygen Reduction to Water. *J. Am. Chem. Soc.* **1996**, *118* (13), 3202–3215.

(36) Richardson, P. F.; Kreilick, R. W. Transition Metal Complexes with Radical Ligands: Pyridyliminonitroxide Radicals with Copper and Vanadium. **1978**, *1*, 285–291.

(37) Eaton, S. S.; More, K. M.; Sawant, B. M.; Boymel, P. M.; Eaton, G. R. Metal-Nitroxyl Interactions. 29. EPR Studies of Spin-Labeled Copper Complexes in Frozen Solution. *J. Magn. Reson.* **1983**, *52* (3), 435–449.

(38) Duboc-Toia, C.; Hassan, A. K.; Mulliez, E.; Ollagnier-de Choudens, S.; Fontecave, M.; Leutwein, C.; Heider, J. Very High-Field EPR Study of Glycyl Radical Enzymes. *J. Am. Chem. Soc.* **2003**, *125* (1), 38–39.

(39) Https://lcced.biocatnet.de/superfamilies.

(40) Winkler, J. R.; Gray, H. B.; Winkler, J. R. Could Tyrosine and Tryptophan Serve Multiple Roles in Biological Redox Processes? *Philos. Trans. R. SOc. A.* **2015**, *373*: 20140178.

(41) Komori, H.; Sugiyama, R.; Kataoka, K.; Miyazaki, K.; Higuchi, Y.; Sakurai, T. New Insights into the Catalytic Active-Site Structure of Multicopper Oxidases. *Acta Crystallogr. Sect. D Biol. Crystallogr.* **2014**, *70* (3), 772–779.